

Article

# The Neutral Voltage Difference Signal as a Means of Investigating Eccentricity and Demagnetization Faults in an AFPM Synchronous Generator

Alexandra C. Barmpatza 

Department of Mechanical Engineering, Hellenic Mediterranean University, 71004 Heraklion, Greece; abarmpatza@hmu.gr; Tel.: +30-694-2479943

**Abstract:** This article investigates the neutral voltage difference signal,  $V_{NO}$  signal, for fault diagnosis. The aforementioned signal is the signal of the voltage between the common star point of the stator and the common star point of the load. The under-study faults are demagnetization and static eccentricity faults, while the machine in which the faults are investigated is an axial flux permanent magnet (AFPM) synchronous generator, suitable for wind power applications. This study was conducted using a 3D finite element method (3D-FEM), and the machine's FEM model was validated through experiments. This method is one of the most accurate methods for electrical machine computation, allowing for a detailed study of electromagnetic behavior. The components that constitute the  $V_{NO}$  signal were determined using a 3D-FEM software program (Opera 18R2). Subsequently, further analysis was performed using MATLAB R2022b software, and a fast Fourier transform (FFT) was applied to this signal. In all the investigated faulty cases, new harmonics appeared, and the healthy amplitudes of most of the already existing harmonics increased. These findings can be used for fault identification. The analysis revealed that the harmonic frequency of  $1.5f_s$  was the most dominant in the case of demagnetization, while in the case of static eccentricity, the most dominant harmonic was a frequency equal to the machine's operating frequency,  $f_s$ . The novelty of this study is that this signal has not previously been used for fault identification, especially in AFPM synchronous machines. This signal depends on EMF voltage and stator phase currents but is less sinusoidal. Consequently, it can detect faults in cases where the aforementioned signals cannot be used for detection.



**Citation:** Barmpatza, A.C. The Neutral Voltage Difference Signal as a Means of Investigating Eccentricity and Demagnetization Faults in an AFPM Synchronous Generator. *Machines* **2023**, *11*, 647. <https://doi.org/10.3390/machines11060647>

Academic Editor: Ahmed Abu-Siada

Received: 30 April 2023

Revised: 30 May 2023

Accepted: 5 June 2023

Published: 14 June 2023



**Copyright:** © 2023 by the author. Licensee MDPI, Basel, Switzerland. This article is an open access article distributed under the terms and conditions of the Creative Commons Attribution (CC BY) license (<https://creativecommons.org/licenses/by/4.0/>).

**Keywords:** demagnetization; eccentricity; fault diagnosis; permanent magnet; synchronous generator

## 1. Introduction

Fault diagnostics is a very important subject in the field of electrical machines, as faults reduce the efficiency and increase the cost of every electromechanical system. The majority of existing studies investigate faults in asynchronous machines, which are the most popular machine type in the industry [1–5]. Regarding synchronous machines, there are also many studies that are dedicated to faults in this machine type. However, these investigations are focused on radial flux synchronous machines (RFSMs), which are a more widespread topology than axial flux synchronous machines (AFSMs). Recently, AFSMs, especially those with topologies containing permanent magnets, have increasingly appeared in the industry, with many applications such as in wind power energy systems, electrical vehicles, ship propulsion, elevators, floppy disk drives, low-torque servomotors, etc. [6–8]. This type of machine presents many advantages compared with conventional RFSMs. AFSMs used in wind energy conversion (WEC) systems provide high output power, high torque, operational ability in a significant speed range, significant reliability, and the opportunity to eliminate the gearbox by adding more magnetic poles in the generator. Indeed, the price of permanent magnets (PMs) is still high; however, a mechanical part such as the gearbox also increases the need for maintenance and the overall cost of the system. In addition,

over time, permanent magnets will become cheaper, which will lead to ever greater use of these machine types, especially for wind power applications.

Nevertheless, in addition to the costs of AFSMs, permanent magnets are composed of rare earth metals and are prone to demagnetization that can be reversible, irreversible, total, or partial. The main cause of demagnetization is machine overheating, which is caused due to either generator operation or heat dissipation problems. Other important causes of demagnetization include various types of physical damage to the magnet, machine aging, the reverse magnetic field that can exist due to a short-circuit fault, manufacturing defects, and corrosion, as well as electrical or mechanical stresses [9–13]. In addition, permanent magnets are fragile materials that can break during their construction or operation. Electrical machines, especially wind generators, often operate in harsh environments under conditions of pollution, humidity, vibration, high temperature, and overload, which are capable of demagnetization faults [9]. In addition, a wind farm can be a costly and difficult procedure, because these farms are often built far from the city center and, in certain cases, also in offshore environments.

Demagnetization faults lead to an asymmetric distribution of the magnetomotive force (MMF), while the magnetic flux is irreversibly reduced and distributed unevenly in the machine. Furthermore, generator efficiency and the induced voltage decrease. However, this fault not only disturbs the symmetry of the airgap magnetic flux density but also affects the stator voltage and current [14]. Additionally, it causes audible noise and vibration in the machine [10,15].

Aside from demagnetization, another important electrical machine fault is eccentricity. Eccentricity is a faulty condition that can be the result of mechanical or thermal stresses, the bending of the rotor during assembly, or imperfect assembly [16]. In this machine type (AFSMs), two cases of eccentricity can occur: angular eccentricity and axial eccentricity. Both create problems for the generator and the overall system because audible noise, vibration, bearing wear, and torque ripple are the main effects of the eccentricity fault. The latter can lead to degraded performance and strain the generator, resulting in a reduced lifespan [17–20]. Especially for AFSMs, in which the overall axial length is shorter than RFSMs, the generator's diameter-to-length ratio is high, a fact that increases the probability of eccentricity [20]. Consequently, studies of this specific fault in AFSMs are very important for the timely diagnosis and repair of the generator.

The most significant studies involving the eccentricity and demagnetization fault diagnosis of AFPM synchronous machines are now discussed. In the study by De Bisschop et al. [21], search coils and an analytical model were utilized for the demagnetization diagnosis of a machine with two rotors and one stator. In both studies conducted by Mirimani et al. [18,19], the static angular eccentricity was investigated, and the proposed method was based on EMF voltage values of the machine's phase coils. In [22], Ajily et al. used a 3D-field reconstruction method for the study of demagnetization faults and the faults of static and dynamic eccentricity. In the study by Lamprokostas et al. [23], an analysis of the instant power spectrum of the generator was carried out for demagnetization diagnosis. In two studies by De Bisschop et al. [24,25], demagnetization was diagnosed using a forward problem for terminal voltage calculation in combination with an analytical model. In [26], Saaverda et al. investigated the demagnetization fault utilizing the stator current, the output torque, and zero-sequence voltage spectra. In another study by De Bisschop et al. [27], a time-harmonic analytical model was used for the identification of both demagnetization and eccentricity faults in a double-rotor-single-stator topology. In [28], Bahador et al. used the flux density and the mean torque for the diagnosis of demagnetization caused by a short-circuit fault. In three studies by Barmpatza et al. [14,29,30], the spectra of the stator current and EMF voltage were used for demagnetization fault identification. In the study by Skarmoutsos et al. [31], dynamic eccentricity was investigated, using a novel algorithm based on the stator current spectrum, while different combinations between slots and poles were taken into account. In [32], Skarmoutsos et al. used a method based on search coils for the diagnosis of

demagnetization, together with angular, axial, static, and dynamic eccentricity. Gyftakis et al. [33] proposed a method based on higher harmonics of the stator current spectrum. The proposed method can separate demagnetization from eccentricity and short-circuit faults while taking into account transient machine conditions. In the study by Haddad et al. [34], the  $V_d$  and  $V_q$  voltage values were used for eccentricity diagnosis. Ogidi et al. [35] proposed a method based on vibration analysis for the detection of static angular eccentricity. In another study by Ogidi et al. [36], static eccentricity and short-circuit faults were separated, using vibration analysis and the stator current spectrum for fault diagnosis. In both studies conducted by Barmpatza et al. [37,38], static angular eccentricity and axial eccentricity faults were studied utilizing the EMF voltage, the stator current, and the sum of the generator's three-phase EMF voltage values. In another study by Ogidi et al. [20], the space harmonics and subharmonics of the current, together with torque ripples, were investigated for static angular eccentricity diagnosis. Guo et al. [39] proposed an analytical method to model a series of manufacturing defects, such as static and dynamic eccentricities, both angular and axial. The magnetic field and the induced voltage waveforms were also studied for fault identification. In the study by Di Gerlando et al. [40], geometrical imperfections were investigated in generators with concentrated coils. The fault impact on the resulting axial force, the bending torques on the shaft, and the circulation current in the winding parallel paths, were taken into account. Huang et al. [41] investigated an AFPM with concentrated winding. An analytical model was proposed, while the back EMF voltage and cogging torque were utilized for the diagnosis of static eccentricity. In the study by Marignetti et al. [42], a quasi-three dimensional model was proposed for eccentricity detection, while the influences of the fault on the airgap density, the cogging torque, and the unbalanced force were studied. Verkroost et al. [43] introduced a fault tolerant deadbeat controller to compensate for demagnetization. Finally, in three studies by Barmpatza et al. [44–46], combined eccentricity and demagnetization faults were investigated.

In this article, static eccentricity and demagnetization faults are investigated in an AFPM synchronous generator, suitable for a wind turbine system. The machine has a single-stator–single-rotor topology, although the results can be extended to AFPMs consisting of more rotors or stators. Firstly, the generator is presented, and its basic characteristics are listed. The results of the experimental verification of the FEM generator model conducted to strengthen the investigation's accuracy are also presented. Subsequently, the proposed  $V_{NO}$  signal is explained and expressed with analytical expressions. From the literature review, which summarizes the most significant studies in AFPM synchronous generators' diagnostics, it is clear that this signal has not previously been used for the detection of demagnetization and eccentricity. Consequently, this investigation is novel and aims to give the scientific community an additional means for fault diagnosis. In this paper, it is also revealed that the neutral voltage difference signal spectrum can distinguish demagnetization from static eccentricity fault. In the Section 3, simulation results are presented. Firstly, partial demagnetization is studied for two fault levels: 20% and 50%. The waveforms and spectra of the proposed signal in healthy and faulty cases are presented. Secondly, two different types of eccentricities, angular and axial, are studied using the  $V_{NO}$  signal and the corresponding spectrum. In the case of static angular eccentricity, faulty cases of levels 30% and 40% are studied. In the case of static axial eccentricity, 1 mm and 2 mm misalignments between the rotor and the stator are taken into account. Finally, the Section 4 highlights the most important findings that emerge from this study, and future goals are also presented.

## 2. Materials and Methods

### 2.1. The AFPM Synchronous Generator

The machine used for fault analysis is an AFPM synchronous generator with a single-stator–single-rotor topology, as shown in Figure 1. The stator is constructed of resin and includes a three-phase, star-connected, trapezoidal winding, consisting of 12 coils. Consequently, each phase has four coils, each consisting of 210 turns. The thickness of the

stator is 18 mm, the generator's external radius is 158 mm, and its internal radius is 60 mm. The machine's airgap thickness is equal to 3 mm, and the rotor has a thickness of 12 mm and contains 16 NdFeB trapezoidal magnets, 8 south and 8 north, of 45N grade. Further basic generator dimensions are listed in [45], except that it involves a double-sided rotor topology generator. However, both the winding and magnet dimensions are the same used in this study, and the only difference is that the second rotor and its magnets were not used in this study. The same study can be extended to a topology with more rotors and stators, which will be a future step of this investigation. Regarding the single-sided rotor topology that is presented here, the nominal speed was 375 rpm, the nominal frequency was 50 Hz, and the nominal voltage was 70 V for a nominal resistive load equal to 30 Ohm. All the above data are also summarized in Table 1, for easier access and observation.

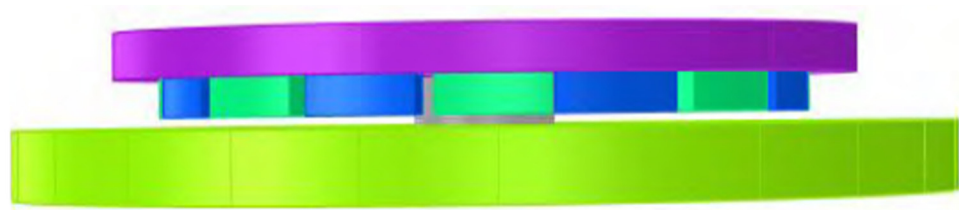


**Figure 1.** The FEM model of the machine in which the faults are studied.

**Table 1.** The generator data.

Nominal Speed	Nominal Frequency	Nominal Voltage	Nominal Load	Number of Coils	Number of Turns per Coil	Number of Poles	Thickness of the Stator	Thickness of the Airgap	Thickness of the Rotor	External Radius	Internal Radius
375 rpm	50 Hz	70 V	30 Ohm	12	210	16	18 mm	3 mm	12 mm	158 mm	60 mm

## 2.2. Experimental Validation of the Generator Model

The aforementioned machine has been constructed in the laboratory [14,23,45], for both single-rotor and double-rotor topologies. Figure 2 illustrates the corresponding experimental setup. The AFPM synchronous generator is driven by a three-phase induction machine, and the experimental values in this study were obtained using a Lab View data acquisition card. Subsequently, the experimental results were further analyzed using MATLAB software. The experimental results related to the generator stator current validated the corresponding values derived from the simulation. Figure 3 depicts the stator current of phase A, which was obtained through experiment and simulation accordingly, for the healthy generator when the speed was 600 rpm, and the machine fed a resistive load equal to 30 Ohm. It can be seen that the two waveforms are very close to each other, a fact that validates the accuracy of the FEM model. More specifically, the error between the two measurements was less than 2%, which is an acceptable error for the simulation validity. For simulation, the generator was designed using the same properties as the real machine. The analysis chosen in Opera 3D software was the transient electromagnetic analysis. In addition, the simulation model contained 3,966,501 elements, and the utilized PC was an Intel computer i7-4770 with 8 GB RAM.

## 2.3. The Proposed Method

The proposed method is based on the fault-related harmonics of the spectrum of the voltage between the common star point of the stator and the common star point of the load. It is commonly known that the sum of three sinusoidal currents with a phase difference of  $120^\circ$  between them when entering a node is zero in every period. When these currents are not purely sinusoidal signals, there are additional harmonics in their spectra besides the fundamental harmonic, and their sum is not zero, as in the case of electric signals of an electrical machine. Consequently, by computing the voltage between the common star point of the stator winding and the common star point of the load, a new signal, the  $V_{NO}$

signal, is generated, which is less sinusoidal than the basic electrical signals of the machine. Therefore, this signal can detect those faults that the spectra of the voltage or current of the generator fail to detect.

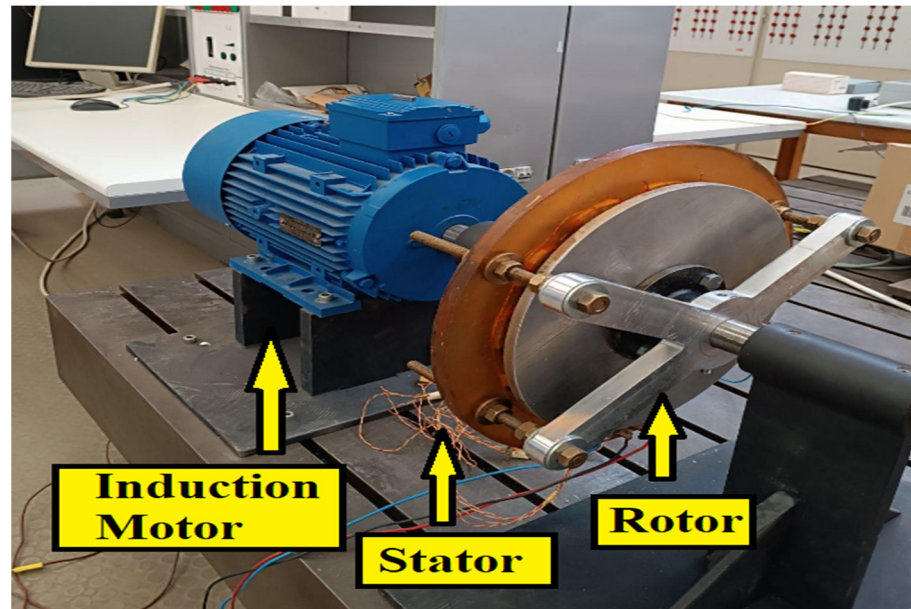


Figure 2. The experimental setup in the laboratory.

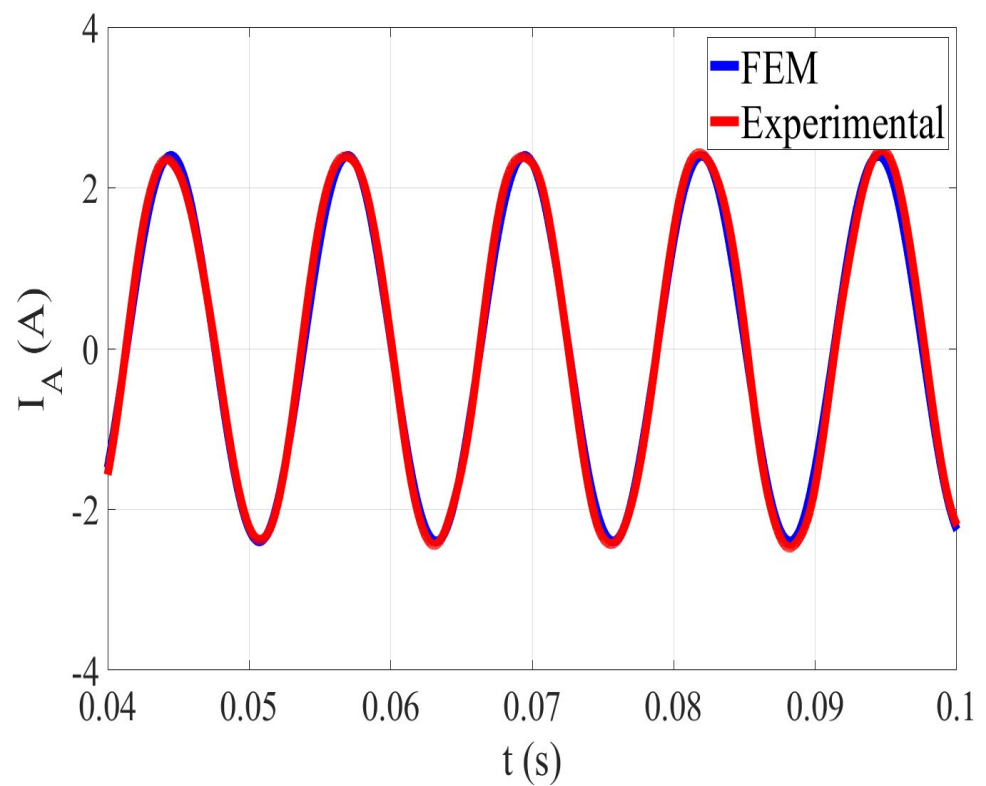
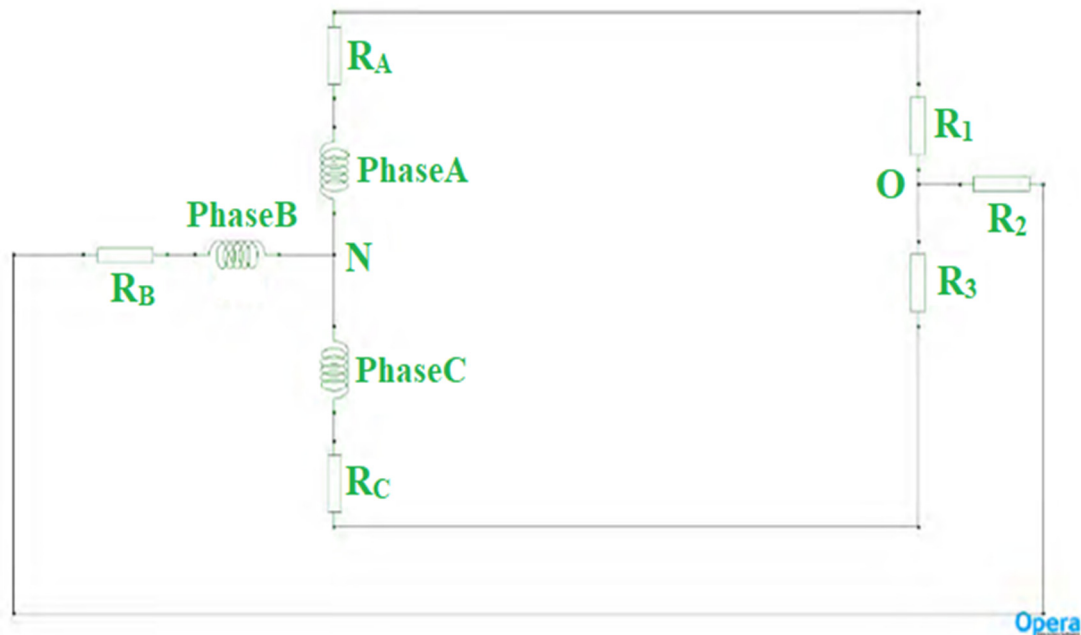


Figure 3. The stator current of phase A in the healthy generator when the speed was 600 rpm and the machine fed a 30 Ohm resistive load: blue line—waveform generated using the FEM model; red line—waveform generated during the experimental procedure.

The  $V_{NO}$  signal is computed below using the three-phase electrical circuit of the generator stator, which is depicted in Figure 4. More specifically, utilizing basic circuit laws, Equation (1) is derived as follows:

$$V_{AN} + V_{BN} + V_{CN} = R_1 I_A + R_2 I_B + R_3 I_C = 0 \quad (1)$$



**Figure 4.** The electrical circuit of the stator of the machine.

Because the generator load is symmetrical, we can write

$$(V_{AO} - V_{NO}) + (V_{BO} - V_{NO}) + (V_{CO} - V_{NO}) = 0 \quad (2)$$

$$(\text{Phase A} - R_A I_A) + (\text{Phase B} - R_B I_B) + (\text{Phase C} - R_C I_C) = 3V_{NO} \quad (3)$$

Consequently, the expression of the  $V_{NO}$  signal is presented as follows:

$$V_{NO} = \frac{\text{Phase A} + \text{Phase B} + \text{Phase C}}{3} - \frac{R_A I_A + R_B I_B + R_C I_C}{3} \quad (4)$$

Considering Equation (4), it is obvious that this signal depends on the EMF voltage and stator phase currents. Consequently, it is a less sinusoidal signal than the aforementioned signals, which enables fault detection even in cases where the EMF voltage signal or stator phase currents cannot provide a solution.

### 3. Results

In this section, the results are presented for two fault types: demagnetization and eccentricity. The analysis was performed keeping the rotor speed constant at 600 rpm; consequently, the machine operating frequency was 80 Hz, and the generator fed a load equal to 30 Ohm, which was the nominal load.

#### 3.1. Demagnetization Fault

Firstly, partial demagnetization was studied, and two faulty cases were simulated. In the first case, one of the sixteen existing magnets on the rotor was 20% demagnetized, while in the second case, this magnet was 50% demagnetized. Figure 5 depicts the  $V_{NO}$  signal waveforms for the healthy case (in blue) and for the two faulty cases (in red). For both

demagnetization cases, the  $V_{NO}$  signal waveform was different from that of the healthy case, and this modification also affected the corresponding spectra. Figure 6 illustrates the spectra of the healthy and two faulty cases, and Table 2 summarizes the most dominant fault-related harmonics. As can be observed from both Figure 6 and Table 2, the harmonic whose amplitude was more affected by demagnetization was that of a frequency of 120 Hz. This harmonic was equal to 3/2 times the operating frequency of the generator ( $f_s$ ), and the increase in the amplitude of this harmonic component in the  $V_{NO}$  signal spectrum can be an indicator of demagnetization. According to our previous publication [14,45], partial demagnetization also generates fault-related harmonics in the spectra of the EMF voltage and stator current, while the axial component of the total magnetic flux density in the case of demagnetization, with one faulty magnet, can be written as in Equation (5):

$$B_{z\_partialdem} = B_{z\_healthy} - \frac{B_{z\_healthy}}{2pV_{dem}} - \sum_{k=1}^{\infty} \frac{2B_{z\_healthy}}{k\pi V_{dem}} \sin\left(\frac{k\pi}{2p}\right) \cos\left(\frac{2k\pi f_s t}{p}\right) \quad (5)$$

where  $B_{z\_healthy}$  is the axial component of the total magnetic flux density in the healthy case,  $p$  is the generator pole pair,  $f_s$  is the generator fundamental frequency, and  $V_{dem}$  is the amplitude immersion of the  $B_{z\_healthy}$  waveform due to the fault. Figure 7 depicts the stator current spectra generated through the experimental procedure for the healthy case and the case with one demagnetized magnet. The faulty harmonics were of frequencies of 40 Hz, 160 Hz, 200 Hz, 280 Hz, and 320 Hz, which validate the above equation.

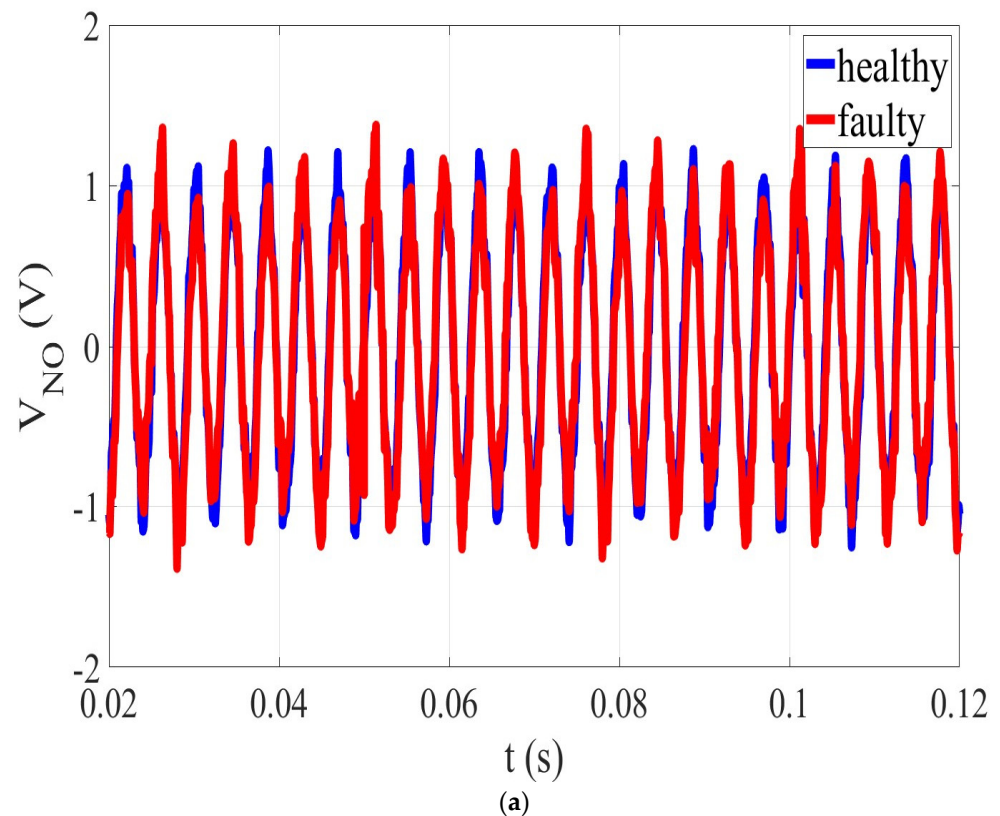
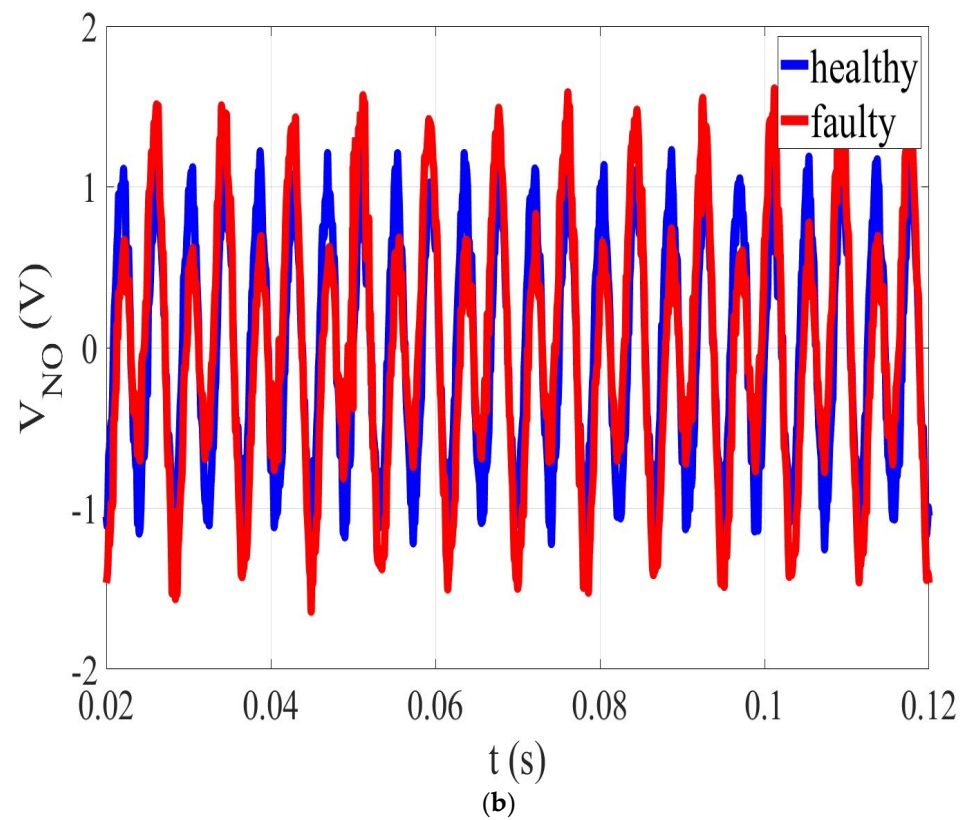
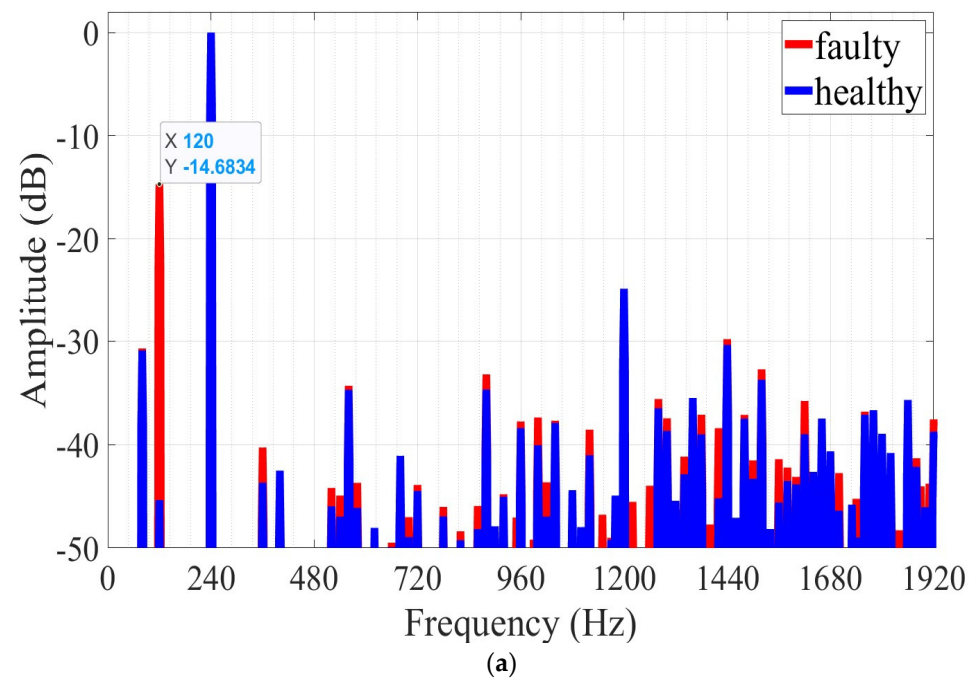


Figure 5. Cont.



**Figure 5.** The  $V_{NO}$  signal waveform for the healthy and faulty cases with (a) 20% partial demagnetization and (b) 50% partial demagnetization.



**Figure 6.** Cont.

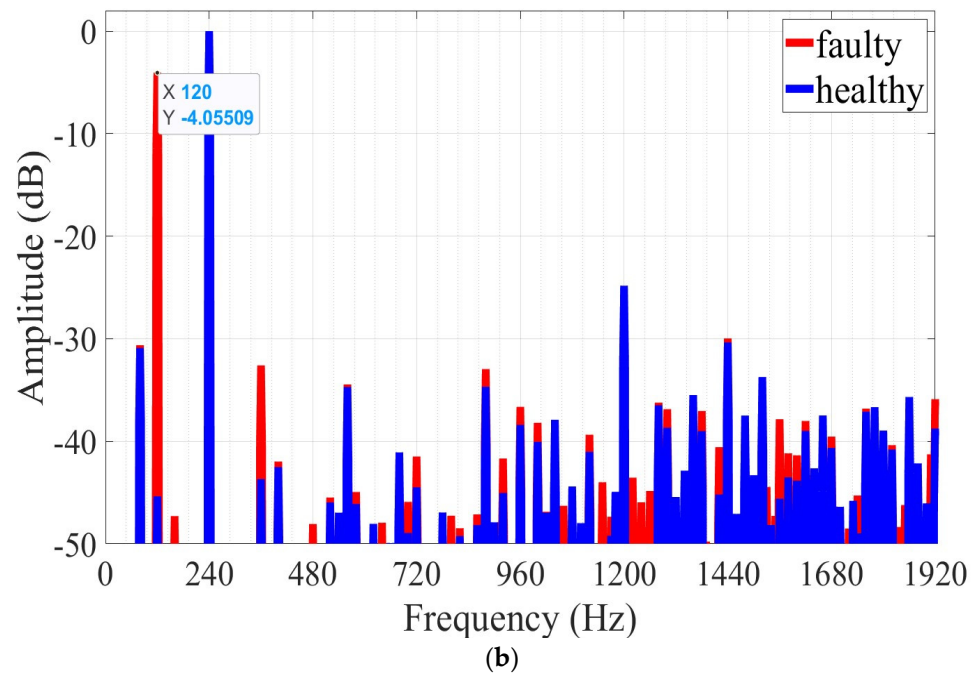


**Figure 6.** The  $V_{NO}$  signal spectra for the healthy and faulty cases with (a) 20% partial demagnetization and (b) 50% partial demagnetization.

**Table 2.** The fault-related harmonics in the  $V_{NO}$  spectrum for partial demagnetization fault.

Frequency (Hz)	Healthy (dB)	20% Partial Demagnetization (dB)	50% Partial Demagnetization (dB)
80	-30.90	-30.9	-30.62
120	-45.35	-14.68	-4.05
360	-43.68	-40.28	-32.60
520	-45.97	-44.19	-45.48
560	-34.70	-34.30	-34.46
580	-46.12	-43.69	-44.94
700	-48.94	-47.01	-45.90
720	-44.48	-43.90	-41.48
820	-49.24	-48.38	-48.48
860	-48.18	-45.93	-47.12
880	-34.68	-33.20	-32.95
920	-45.04	-44.80	-41.67
960	-38.40	-37.76	-36.64
1000	-40.05	-37.38	-38.20
1120	-41.03	-38.55	-39.36
1150	-	-46.78	-43.99
1220	-	-43.53	-43.54
1260	-	-43.98	-44.83
1280	-36.48	-35.59	-36.23
1300	-38.67	-37.45	-36.87
1380	-39.00	-37.11	-37.05
1420	-45.19	-38.41	-40.56
1560	-45.59	-41.41	-37.84
1580	-43.51	-42.22	-41.17
1600	-43.84	-43.12	-41.36

Table 2. Cont.

Frequency (Hz)	Healthy (dB)	20% Partial Demagnetization (dB)	50% Partial Demagnetization (dB)
1620	−38.99	−35.77	−38.02
1740	−48.97	−45.24	−45.28
1840	-	−48.28	−48.36
1850	-	−48.28	−46.21
1920	−38.76	−37.56	−35.89

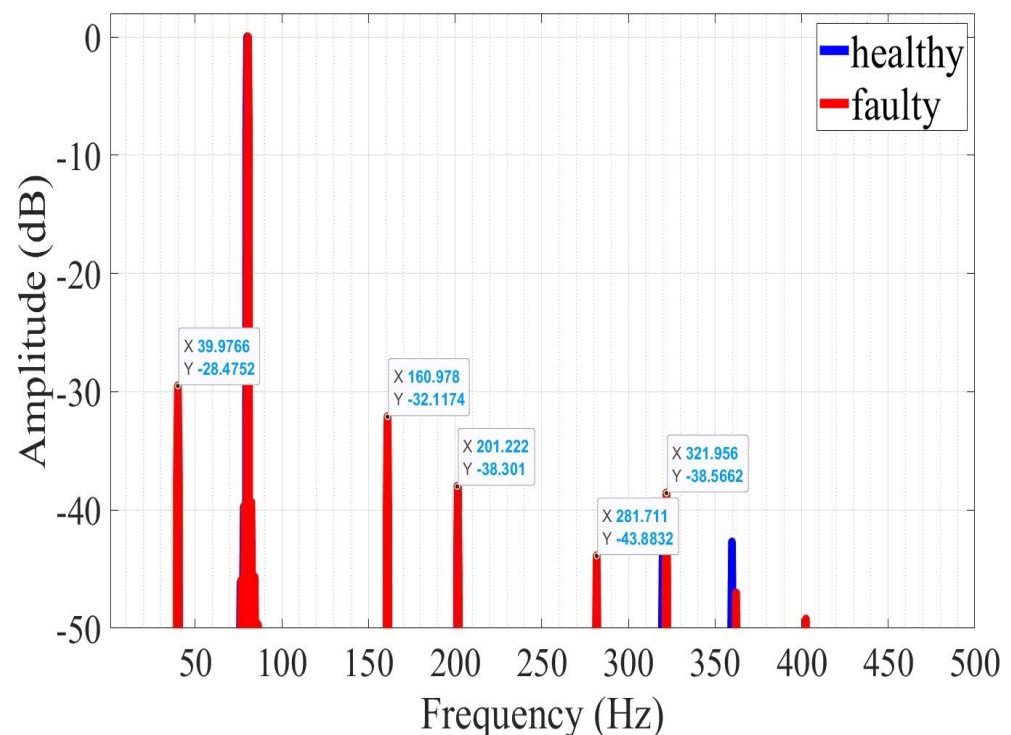


**Figure 7.** The stator current spectra for the healthy case and the case where one magnet was demagnetized generated during the experimental procedure.

### 3.2. Eccentricity Fault

In this section, the eccentricity fault is investigated, and two different types of eccentricity are studied: (a) the static angular eccentricity and (b) the static axial eccentricity. Generally speaking, static eccentricity is a case in which the rotor axis coincides with the rotational axis but does not coincide with the stator axis. Figure 8 presents schematic diagrams that explain the two types of eccentricity. As seen in this figure, in the first type, the rotor is displaced relative to the stator by a certain angle, while in the second case, the rotor offsets from the stator by some millimeters.

#### 3.2.1. Angular Eccentricity Fault

Firstly, the static angular eccentricity fault was investigated, and more specifically, two different levels of the fault were considered: 30% and 40%. The healthy and faulty waveforms of the  $V_{NO}$  signal are depicted in Figure 9. Similar to the case of partial demagnetization, the static angular eccentricity fault distorts the  $V_{NO}$  signal waveform. This distortion results in faulty spectra with new harmonics related to the fault. According to our previous study [37], the static angular eccentricity in a single-sided rotor AFPM synchronous generator does not generate new harmonics in the spectra of either the EMF voltage or stator current individually. However, as shown in Figure 10, which depicts

the  $V_{NO}$  signal spectrum, a signal depending on both the EMF voltage and stator phase currents, new harmonics related to the fault were generated compared with the healthy case. In both 30% and 40% static angular eccentricity faulty cases, the harmonic whose amplitude changed more with the fault was the harmonic of a frequency of 80 Hz. The frequency of this harmonic is equal to the operating generator frequency, considering the rotor speed of 600 rpm. The above findings are also presented in Table 3, which summarizes the most important fault-related harmonics in the  $V_{NO}$  signal spectrum. It can be seen that, except for the noticeable variation in the harmonic component at 80 Hz, there were also other harmonic components on the  $V_{NO}$  signal spectrum whose amplitudes increased in the case of static angular eccentricity compared with the healthy case. Finally, the amplitude of the 120 Hz harmonic component, which appeared with high amplitude in the case of demagnetization, remained approximately constant in the case of static angular eccentricity.

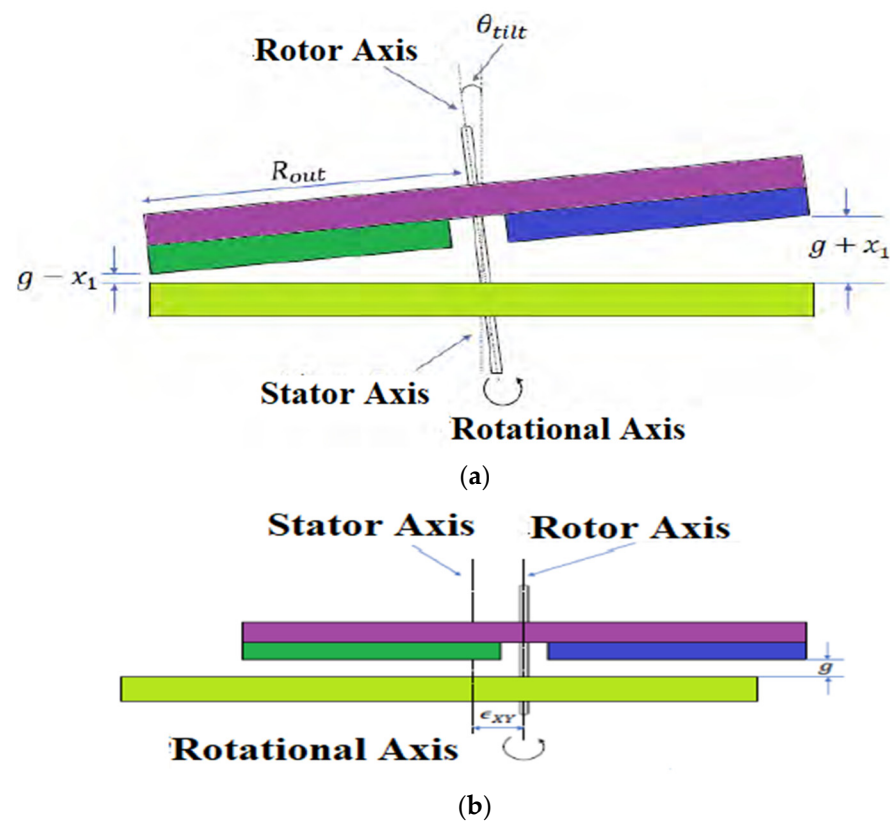


**Figure 8.** Schematic diagram of static eccentricity: (a) angular; (b) axial.

### 3.2.2. Axial Eccentricity Fault

Subsequently, the static axial eccentricity fault was studied for two different levels of rotor–stator offset: 1 mm and 2 mm. Figure 11 shows the  $V_{NO}$  signal waveforms for the healthy case, depicted with blue color, and the two faulty cases, depicted with red color in Figure 11a,b, accordingly. As with the previously examined faulty cases, in this faulty case, the  $V_{NO}$  signal waveforms appear distorted, and fault-related harmonics exist in the corresponding spectra, as depicted in Figure 12. It can be observed that the fault generated new harmonics, and the amplitudes of most of the already existing harmonics in the healthy case increased, as can be seen in Table 4. In this eccentricity type, the harmonic component whose amplitude was affected more by the fault was also that of frequency 80 Hz, which was equal to the generator’s operating frequency. In addition, like in the case of static angular eccentricity, the harmonic component of a frequency of 120 Hz, which was  $3/2$  times the generator’s operating frequency, did not present a noticeable variation.

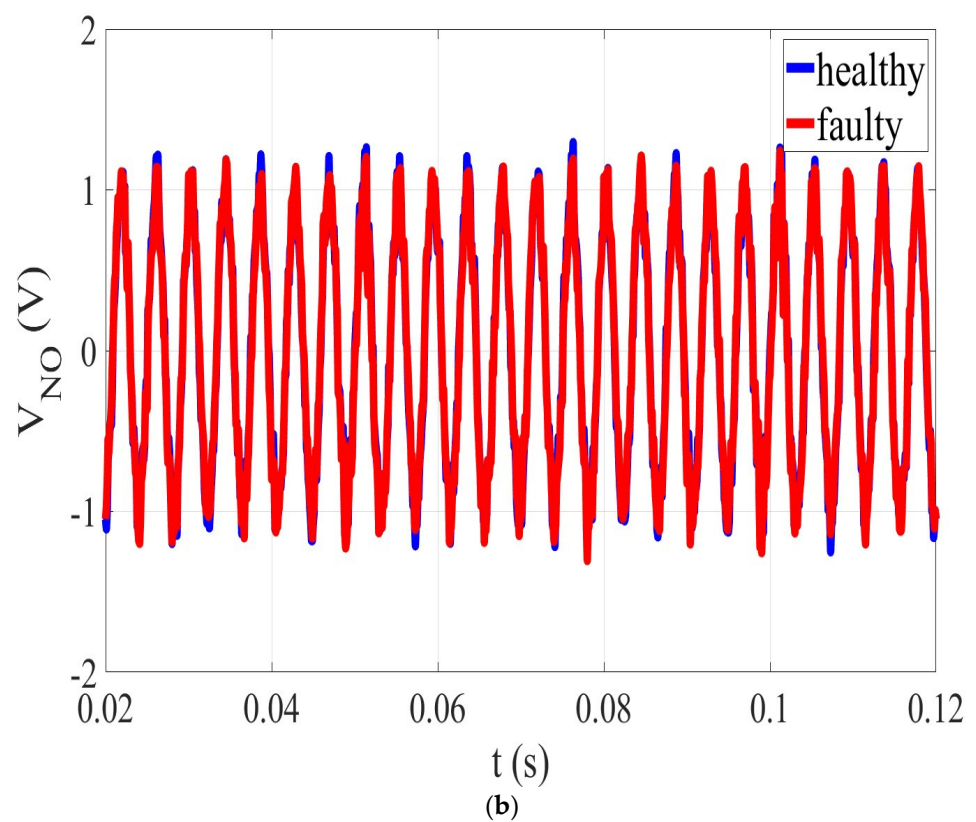
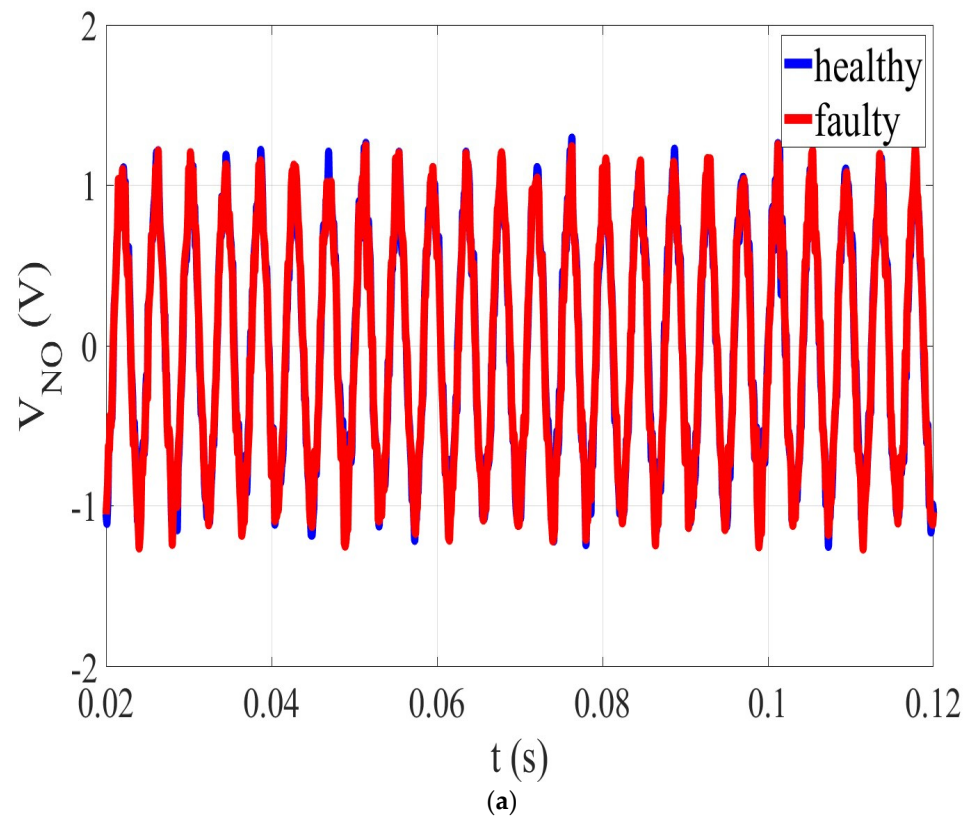
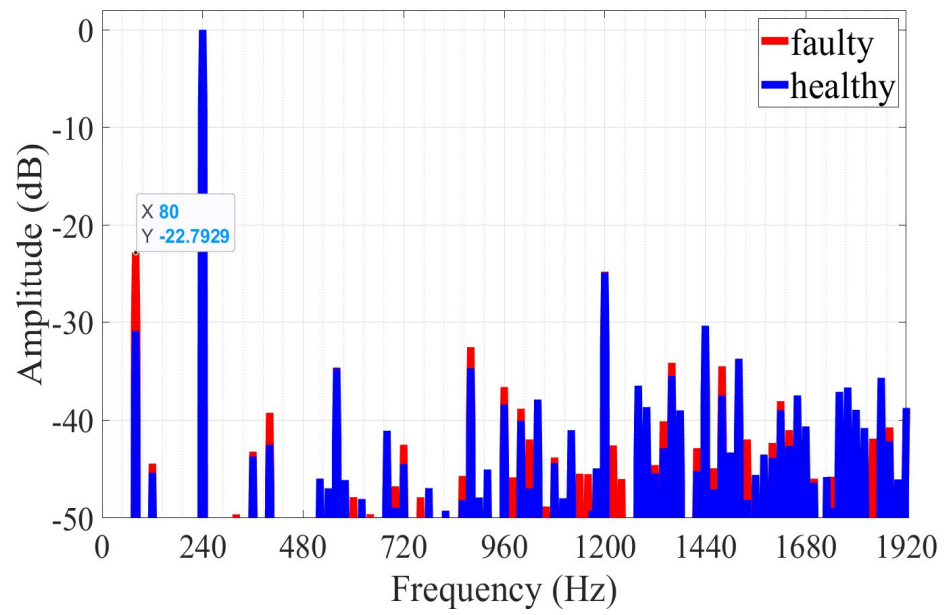
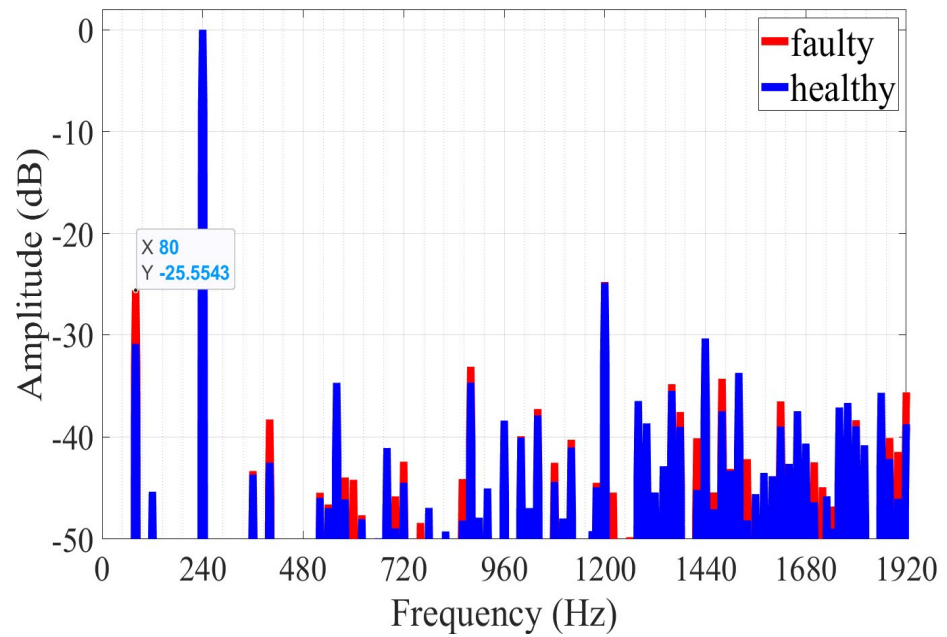


**Figure 9.** The  $V_{NO}$  signal waveform for the healthy and faulty cases with (a) 30% static angular eccentricity and (b) 40% static angular eccentricity.



(a)



(b)

**Figure 10.** The  $V_{NO}$  signal spectra for the healthy and faulty cases with (a) 30% static angular eccentricity and (b) 40% static angular eccentricity.

**Table 3.** The fault-related harmonics in the  $V_{NO}$  spectrum for a static angular eccentricity fault.

Frequency (Hz)	Healthy (dB)	30% Angular Eccentricity (dB)	40% Angular Eccentricity (dB)
80	-30.90	-22.79	-25.55
360	-43.68	-43.21	-43.33
400	-42.51	-39.25	-38.29
600	-	-47.86	-44.19
700	-48.94	-46.75	-45.81

Table 3. Cont.

Frequency (Hz)	Healthy (dB)	30% Angular Eccentricity (dB)	40% Angular Eccentricity (dB)
720	-44.48	-42.51	-42.42
760	-	-47.87	-48.41
860	-48.18	-45.70	-44.12
880	-34.68	-32.55	-33.13
1000	-40.05	-38.83	-39.93
1080	-44.40	-43.82	-42.52
1220	-	-42.58	-45.44
1360	-35.48	-34.14	-34.84
1420	-45.19	-42.86	-40.13
1460	-47.07	-44.91	-45.42
1480	-37.49	-34.50	-34.30
1540	-48.16	-41.97	-42.17
1620	-38.99	-38.06	-36.52
1700	-46.38	-45.97	-42.47
1880	-42.15	-40.74	-40.10

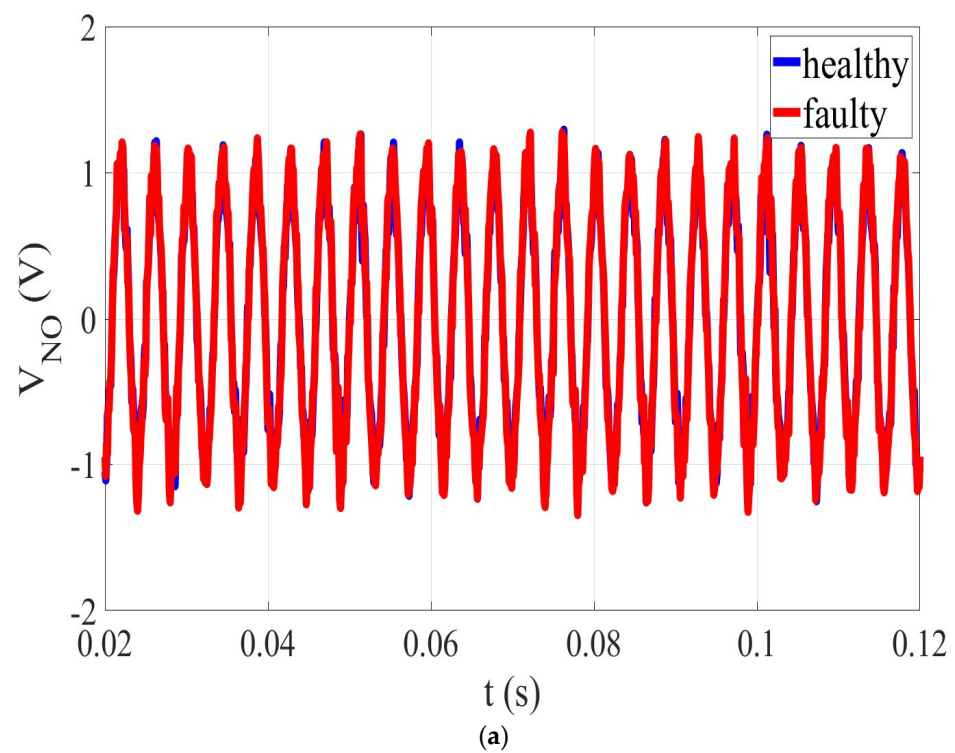
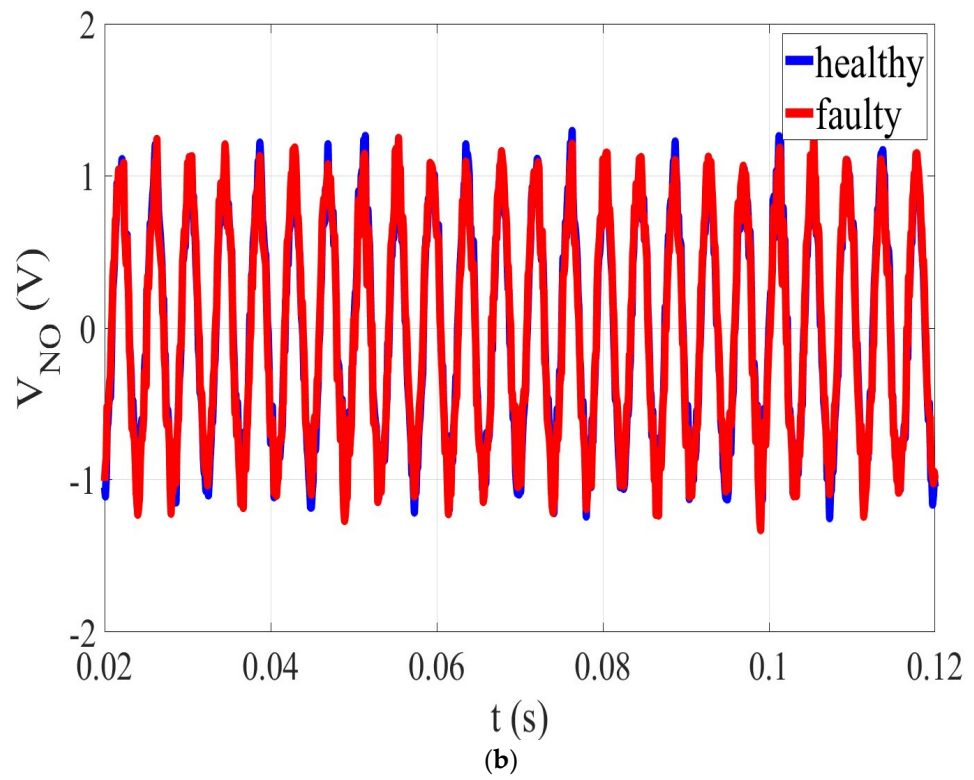
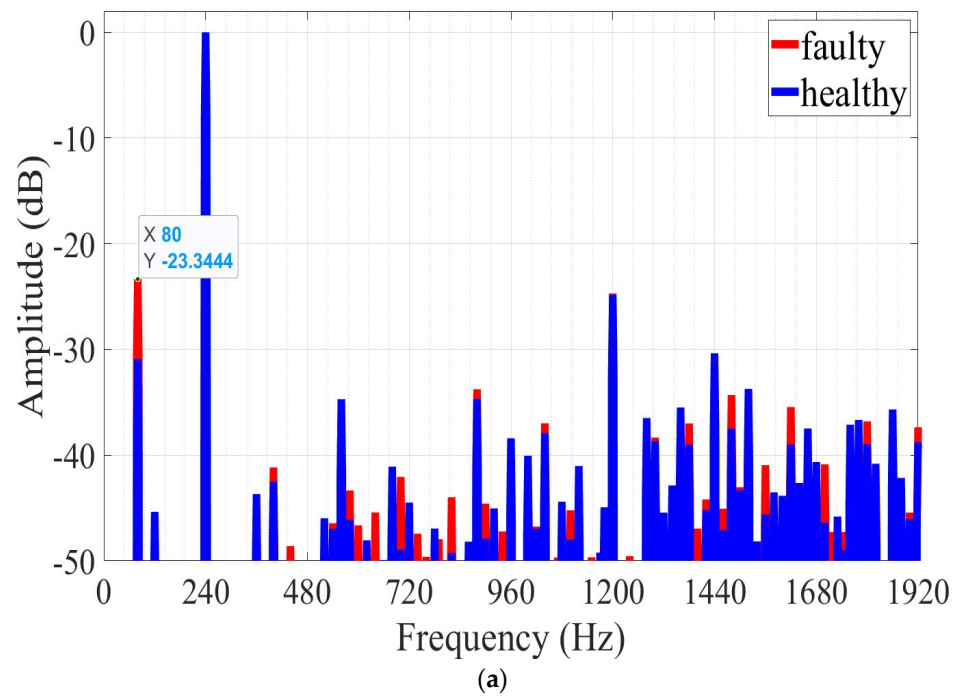


Figure 11. Cont.



**Figure 11.** The  $V_{NO}$  signal waveform for the healthy and faulty cases with (a) 1 mm static axial eccentricity and (b) 2 mm static axial eccentricity.



**Figure 12.** Cont.

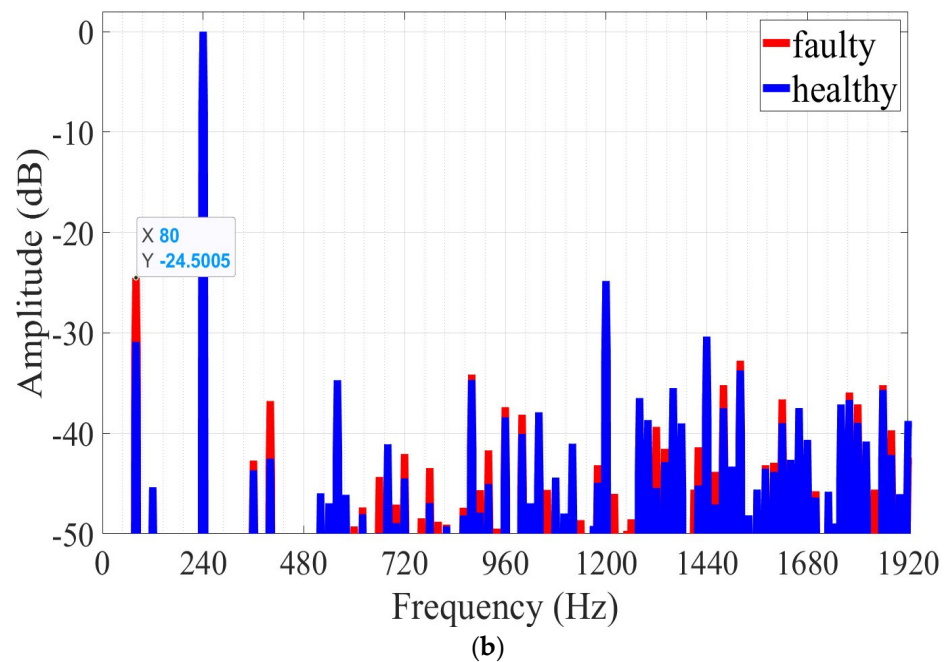


**Figure 12.** The  $V_{NO}$  signal spectra for the healthy and faulty cases with (a) 1 mm static axial eccentricity and (b) 2 mm static axial eccentricity.

**Table 4.** The fault-related harmonics in the  $V_{NO}$  spectrum for a static axial eccentricity fault.

Frequency (Hz)	Healthy (dB)	1 mm Axial Eccentricity (dB)	2 mm Axial Eccentricity (dB)
80	-30.90	-23.34	-24.50
400	-42.51	-41.16	-36.77
600	-	-46.63	-49.26
700	-48.94	-42.06	-47.09
760	-	-49.61	-48.44
880	-34.68	-33.79	-34.14
900	-47.89	-44.59	-45.65
940	-	-47.21	-49.47
1420	-45.19	-44.19	-41.38
1460	-47.07	-45.07	-43.83
1480	-37.49	-34.31	-35.19
1620	-38.99	-35.44	-36.62
1700	-46.38	-40.86	-45.76
1800	-38.94	-36.80	-37.10

In other words, an increased amplitude, compared with the healthy case, of the harmonic component whose frequency equaled  $3/2$  of the generator's operation frequency ( $f_s$ ) in the  $V_{NO}$  signal spectrum indicated demagnetization. Accordingly, an increased amplitude of the harmonic component whose frequency equaled the generator's operation frequency ( $f_s$ ) indicated eccentricity.

#### 4. Discussion

In this study, demagnetization and static eccentricity faults, both angular and axial, were investigated in a single-stator–single-rotor AFPM synchronous machine. Both the healthy and faulty machine models were simulated with 3D-FEM, and the stator current and the generator's voltage values were determined. Utilizing these values, a new signal, the  $V_{NO}$  voltage signal, was generated and analyzed. Using MATLAB software, this novel signal, which was the signal of the voltage between the common star point of the stator and

the common star point of the load, was generated, and by applying FFT, the corresponding spectrum was plotted.

Six faulty cases were simulated in 3D-FEM software, and the signals and spectra of the  $V_{NO}$  voltage were studied. The first two cases concerned demagnetization of 20% and 50%, the second involved the static angular eccentricity of 30% and 40%, and the third involved static axial eccentricity with 1 mm and 2 mm offset. In all cases, the rotor speed was kept constant at 600 rpm, and the generator fed a 30 Ohm resistive load. In addition, the simulated generator model was validated by comparing the stator current waveform of phase A derived from FEM with those of the real machine.

In all the simulated faulty cases, the  $V_{NO}$  voltage waveform appeared distorted compared with the healthy case, while the corresponding spectra were also distorted. The amplitudes of the majority of the harmonics already existing in the healthy case increased, while new harmonics appeared in the spectrum of the  $V_{NO}$  voltage signal. In the case of demagnetization, the harmonic whose amplitude increased more was of a frequency of 120 Hz, or, in other words,  $3/2$  times the generator's operating frequency ( $f_s$ ). This harmonic component did not appear with increased amplitude in the case of angular or axial static eccentricity. In both angular and axial static eccentricity, the harmonic whose amplitude presented the greatest increment was of a frequency of 80 Hz. In other words, the frequency of this harmonic component equaled the operating frequency of the machine and did not appear at a high amplitude in the case of demagnetization. Consequently, it can be assumed that the increase in the harmonic component of a frequency of  $3/2 f_s$  could indicate demagnetization, whereas the increase in the harmonic component of frequency  $f_s$  could indicate static eccentricity. A future goal of this study is to implement the same method in the cases of combined demagnetization and eccentricity faults and in the detection procedure of other fault types.

The investigation of the  $V_{NO}$  voltage signal and its spectrum, especially in an AFPM machine, is one of the novelties of this study. The study reveals a new diagnostic means with which demagnetization and eccentricity can be detected in cases where other means, such as the EMF voltage spectrum or the stator current spectrum, cannot be used for detection. The  $V_{NO}$  voltage signal depends on the EMF voltage and stator phase currents, and it is less sinusoidal and thus more reliable in detecting faults that the aforementioned signals cannot identify.

To conclude, timely and accurate fault diagnosis is very important, especially when the generator will be used in wind power energy production, and for that reason, scientific and technical communities need more and more tools for fault diagnosis. It is commonly known that wind turbines are often built in isolated places and therefore pose difficulties in accessing them in the event of a fault. Therefore, on-time fault detection and diagnosis are very important factors that will increase the reliability and efficiency of the system. Every fault not only demands financial resources for system repair but also reduces the income of each investment in case of a system pause.

**Funding:** This research received no external funding.

**Acknowledgments:** The author would like to thank the Laboratory of Electromechanical Energy Conversion at the University of Patras, for providing access to its facilities, to conduct my simulations using the Opera software. In addition, the author would like to acknowledge the contribution of Joya Kappatou for her work in designing and constructing the AFPMSG, which was used as the studied machine for the fault analysis.

**Conflicts of Interest:** The author declares no conflict of interest.

## References

1. Hyun, D.; Lee, S.; Hong, J.; Bin Lee, S.; Nandi, S. Detection of Airgap Eccentricity for Induction Motors Using the Single-Phase Rotation Test. *IEEE Trans. Energy Convers.* **2012**, *27*, 689–696. [\[CrossRef\]](#)
2. Siddique, A.; Yadava, G.S.; Singh, B. A Review of Stator Fault Monitoring Techniques of Induction Motors. *IEEE Trans. Energy Convers.* **2005**, *20*, 106–114. [\[CrossRef\]](#)

3. Atta, M.E.E.D.; Ibrahim, D.K.; Gilany, M.I. Broken Bar Fault Detection and Diagnosis Techniques for Induction Motors and Drives: State of the Art. *IEEE Access* **2022**, *10*, 88504–88526. [[CrossRef](#)]
4. Filippetti, F.; Franceschini, G.; Tassoni, C.; Vas, P. Recent Developments of Induction Motor Drives Fault Diagnosis Using AI Techniques. *IEEE Trans. Ind. Electron.* **2000**, *47*, 994–1004. [[CrossRef](#)]
5. Sunal, C.E.; Dyo, V.; Velisavljevic, V. Review of Machine Learning Based Fault Detection for Centrifugal Pump Induction Motors. *IEEE Access* **2022**, *10*, 71344–71355. [[CrossRef](#)]
6. Kahourzade, S.; Member, S.; Mahmoudi, A. A Comprehensive Review of Axial-Flux Permanent-Magnet Machines Revue de Littérature Sur Les Machines à Aimant Permanent à Flux Axiale. *Can. J. Electr. Comput. Eng.* **2014**, *37*, 19–33. [[CrossRef](#)]
7. Lee, C.H.T.; Chau, K.T.; Liu, C.; Ching, T.W.; Li, F. A High-Torque Magnetless Axial-Flux Doubly Salient Machine for in-Wheel Direct Drive Applications. *IEEE Trans. Magn.* **2014**, *50*, 1–5. [[CrossRef](#)]
8. Zhao, J.; Quan, X.; Sun, X.; Lin, M.; Niu, S. Influence of Rotor-Pole Number on Electromagnetic Performance of Novel Double-Rotor Hybrid Excited Axial Switched-Flux Permanent-Magnet Machines for EV/HEV Applications. *IEEE Trans. Magn.* **2020**, *56*, 1–6. [[CrossRef](#)]
9. Ullah, Z.; Hur, J. A Comprehensive Review of Winding Short Circuit Fault and Irreversible Demagnetization Fault Detection in PM Type Machines. *Energies* **2018**, *11*, 3309. [[CrossRef](#)]
10. Choi, S.; Haque, M.S.; Tarek, M.T.B.; Mulpuri, V.; Duan, Y.; Das, S.; Garg, V.; Ionel, D.M.; Masrur, M.A.; Mirafzal, B.; et al. Fault Diagnosis Techniques for Permanent Magnet AC Machine and Drives-A Review of Current State of the Art. *IEEE Trans. Transp. Electr.* **2018**, *4*, 444–463. [[CrossRef](#)]
11. Goktas, T.; Zafarani, M.; Akin, B. Discernment of Broken Magnet and Static Eccentricity Faults in Permanent Magnet Synchronous Motors. *IEEE Trans. Energy Convers.* **2016**, *31*, 578–587. [[CrossRef](#)]
12. Henao, H.; Capolino, G.A.; Fernandez-Cabanas, M.; Filippetti, F.; Bruzzese, C.; Strangas, E.; Pusca, R.; Estima, J.; Riera-Guasp, M.; Hedayati-Kia, S. Trends in Fault Diagnosis for Electrical Machines: A Review of Diagnostic Techniques. *IEEE Ind. Electron. Mag.* **2014**, *8*, 31–42. [[CrossRef](#)]
13. Moon, S.; Jeong, H.; Lee, H.; Kim, S.W. Detection and Classification of Demagnetization and Interturn Short Faults of IPMSMs. *IEEE Trans. Ind. Electron.* **2017**, *64*, 9433–9441. [[CrossRef](#)]
14. Barmpatza, A.C.; Kappatou, J.C. Study of the Total Demagnetization Fault of an AFPM Wind Generator. *IEEE Trans. Energy Convers.* **2021**, *36*, 725–736. [[CrossRef](#)]
15. Duan, Y.; Toliyat, H. A Review of Condition Monitoring and Fault Diagnosis for Permanent Magnet Machines. In Proceedings of the 2012 IEEE Power and Energy Society General Meeting, San Diego, CA, USA, 22–26 July 2012; pp. 9–12. [[CrossRef](#)]
16. Thiele, M.; Heins, G. Computationally Efficient Method for Identifying Manufacturing Induced Rotor and Stator Misalignment in Permanent Magnet Brushless Machines. *IEEE Trans. Ind. Appl.* **2016**, *52*, 3033–3040. [[CrossRef](#)]
17. Ogidi, O.O.; Barendse, P.S.; Khan, M.A. Detection of Static Eccentricities in Axial-Flux Permanent-Magnet Machines with Concentrated Windings Using Vibration Analysis. *IEEE Trans. Ind. Appl.* **2015**, *51*, 4425–4434. [[CrossRef](#)]
18. Mirimani, S.M.; Vahedi, A.; Marignetti, F.; Di Stefano, R. An Online Method for Static Eccentricity Fault Detection in Axial Flux Machines. *IEEE Trans. Ind. Electron.* **2015**, *62*, 1931–1942. [[CrossRef](#)]
19. Mirimani, S.M.; Vahedi, A.; Marignetti, F. Effect of Inclined Static Eccentricity Fault in Single Stator-Single Rotor. *IEEE Trans. Magn.* **2012**, *48*, 143–149. [[CrossRef](#)]
20. Ogidi, O.O.; Barendse, P.S.; Khan, M.A. Influence of Rotor Topologies and Cogging Torque Minimization Techniques in the Detection of Static Eccentricities in Axial-Flux Permanent-Magnet Machine. *IEEE Trans. Ind. Appl.* **2017**, *53*, 161–170. [[CrossRef](#)]
21. De Bisschop, J.; Vansompel, H.; Sergeant, P.; Dupré, L. Demagnetization Fault Detection in Axial Flux PM Machines by Using Sensing Coils and an Analytical Model. *IEEE Trans. Magn.* **2017**, *53*, 1–4. [[CrossRef](#)]
22. Ajily, E.; Ardebili, M.; Abbaszadeh, K. Magnet Defect and Rotor Eccentricity Modeling in Axial-Flux Permanent-Magnet Machines via 3-D Field Reconstruction Method. *IEEE Trans. Energy Convers.* **2016**, *31*, 486–495. [[CrossRef](#)]
23. Lamprokostopoulos, A.; Mitronikas, E.; Barmpatza, A. Detection of Demagnetization Faults in Axial Flux Permanent-Magnet Synchronous Wind Generators. *Energies* **2022**, *15*, 3220. [[CrossRef](#)]
24. De Bisschop, J.; Abdallah, A.; Sergeant, P.; Dupre, L. Identification of Demagnetization Faults in Axial Flux Permanent Magnet Synchronous Machines Using an Inverse Problem Coupled with an Analytical Model. *IEEE Trans. Magn.* **2014**, *50*, 1–4. [[CrossRef](#)]
25. De Bisschop, J.; Abdallah, A.A.E.; Sergeant, P.; Dupré, L. Analysis and Selection of Harmonics Sensitive to Demagnetisation Faults Intended for Condition Monitoring of Double Rotor Axial Flux Permanent Magnet Synchronous Machines. *IET Electr. Power Appl.* **2018**, *12*, 486–493. [[CrossRef](#)]
26. Saavedra, H.; Riba, J.R.; Romeral, L. Magnet Shape Influence on the Performance of AFPMM with Demagnetization. In Proceedings of the IECON 2013—39th Annual Conference of the IEEE Industrial Electronics Society, Vienna, Austria, 10–13 November 2013; pp. 973–977. [[CrossRef](#)]
27. De Bisschop, J.; Sergeant, P.; Hemeida, A.; Vansompel, H.; Dupré, L. Analytical Model for Combined Study of Magnet Demagnetization and Eccentricity Defects in Axial Flux Permanent Magnet Synchronous Machines. *IEEE Trans. Magn.* **2017**, *53*, 1–12. [[CrossRef](#)]
28. Bahador, N.; Darabi, A.; Hasanabadi, H. Demagnetization Analysis of Axial Flux Permanent Magnet Motor under Three Phase Short Circuit Fault. In Proceedings of the PEDSTC 2013—4th Annual International Power Electronics, Drive Systems and Technologies Conference, Tehran, Iran, 13–14 February 2013; pp. 333–337. [[CrossRef](#)]

29. Barmpatza, A.C.; Kappatou, J.C. Demagnetization Faults Detection in an Axial Flux Permanent Magnet Synchronous Generator. In Proceedings of the 2017 IEEE 11th International Symposium on Diagnostics for Electrical Machines, Power Electronics and Drives (SDEMPED), Tinos, Greece, 29 August–1 September 2017; pp. 153–159. [\[CrossRef\]](#)
30. Barmpatza, A.C.; Kappatou, J.C. Study of the Demagnetization Fault in an AFPM Machine in Relation with the Magnet Location. In Proceedings of the 2018 XIII International Conference on Electrical Machines (ICEM), Alexandroupoli, Greece, 3–6 September 2018; pp. 1952–1958. [\[CrossRef\]](#)
31. Skarmoutsos, G.A.; Gyftakis, K.N.; Mueller, M. Analytical Prediction of the MCSA Signatures Under Dynamic Eccentricity in PM Machines With Concentrated Non-Overlapping Windings. *IEEE Trans. Energy Convers.* **2022**, *37*, 1011–1019. [\[CrossRef\]](#)
32. Skarmoutsos, G.A.; Gyftakis, K.N.; Mueller, M.A. A New Approach to PM Machine Fault Diagnostics Using Two Magnetically-Coupled Search-Coils. In Proceedings of the 2022 International Conference on Electrical Machines (ICEM), Valencia, Spain, 5–8 September 2022; pp. 1616–1621. [\[CrossRef\]](#)
33. Gyftakis, K.N.; Garcia-Calva, T.A.; Skarmoutsos, G.A.; Morinigo-Sotelo, D.; Mueller, M.; Romero-Troncoso, R.d.J. Demagnetization Monitoring and Identification in PM Generators With Concentrated Windings During Transient Conditions. *IEEE Trans. Ind. Appl.* **2022**, *59*, 1510–1518. [\[CrossRef\]](#)
34. Haddad, R.Z. Detection and Identification of Rotor Faults in Axial Flux Permanent Magnet Synchronous Motors Due to Manufacturing and Assembly Imperfections. *IEEE Trans. Energy Convers.* **2020**, *35*, 174–183. [\[CrossRef\]](#)
35. Ogidi, O.O.; Barendse, P.S.; Khan, M.A. Detection of Static Eccentricity Faults in AFPM Machine with Asymmetric Windings Using Vibration Analysis. In Proceedings of the 2014 International Conference on Electrical Machines (ICEM), Berlin, Germany, 2–5 September 2014; pp. 1549–1554. [\[CrossRef\]](#)
36. Ogidi, O.O.; Barendse, P.S.; Khan, M.A. Fault Diagnosis and Condition Monitoring of Axial-Flux Permanent Magnet Wind Generators. *Electr. Power Syst. Res.* **2016**, *136*, 1–7. [\[CrossRef\]](#)
37. Barmpatza, A.C.; Kappatou, J.C.; Skarmoutsos, G.A. Investigation of Static Angular and Axis Misalignment in an AFPM Generator. In Proceedings of the 2019 IEEE Workshop on Electrical Machines Design, Control and Diagnosis (WEMDCD), Athens, Greece, 22–23 April 2019; pp. 163–168. [\[CrossRef\]](#)
38. Barmpatza, A.C.; Kappatou, J.C. A Study of Static Angular and Axis Eccentricity in a Double-Sided Rotor AFPM Generator Using 3D-FEM. In Proceedings of the 2019 IEEE 12th International Symposium on Diagnostics for Electrical Machines, Power Electronics and Drives (SDEMPED), Toulouse, France, 27–30 August 2019; pp. 94–100. [\[CrossRef\]](#)
39. Guo, B.; Huang, Y.; Peng, F.; Guo, Y.; Zhu, J. Analytical Modeling of Manufacturing Imperfections in Double-Rotor Axial Flux PM Machines: Effects on Back EMF. *IEEE Trans. Magn.* **2017**, *53*, 5090. [\[CrossRef\]](#)
40. Di Gerlando, A.; Foglia, G.M.; Iacchetti, M.F.; Perini, R. Effects of Manufacturing Imperfections in Concentrated Coil Axial Flux PM Machines: Evaluation and Tests. *IEEE Trans. Ind. Electron.* **2014**, *61*, 5012–5024. [\[CrossRef\]](#)
41. Huang, Y.; Guo, B.; Hemeida, A.; Sergeant, P. Analytical Modeling of Static Eccentricities in Axial Flux Permanent-Magnet Machines with Concentrated Windings. *Energies* **2016**, *9*, 892. [\[CrossRef\]](#)
42. Marignetti, F.; Vahedi, A.; Mirimani, S.M. An Analytical Approach to Eccentricity in Axial Flux Permanent Magnet Synchronous Generators for Wind Turbines. *Electr. Power Compon. Syst.* **2015**, *43*, 1039–1050. [\[CrossRef\]](#)
43. Verkroost, L.; De Bisschop, J.; Vansompel, H.; De Belie, F.; Sergeant, P. Active Demagnetization Fault Compensation for Axial Flux Permanent-Magnet Synchronous Machines Using an Analytical Inverse Model. *IEEE Trans. Energy Convers.* **2020**, *35*, 591–599. [\[CrossRef\]](#)
44. Barmpatza, A.C.; Kappatou, J.C. Investigation of the Combined Eccentricity and Demagnetization Fault in an AFPMSG. In Proceedings of the 2020 International Conference on Electrical Machines (ICEM), Gothenburg, Sweden, 23–26 August 2020; pp. 1377–1383. [\[CrossRef\]](#)
45. Barmpatza, A.C.; Kappatou, J.C. Study of a Combined Demagnetization and Eccentricity Fault in an AFPM Synchronous Generator. *Energies* **2020**, *13*, 5609. [\[CrossRef\]](#)
46. Barmpatza, A.C.; Kappatou, J.C. Fault Diagnosis in an AFPM Synchronous Generator through Phase EMF Voltage Sum. In Proceedings of the 2021 IEEE 13th International Symposium on Diagnostics for Electrical Machines, Power Electronics and Drives (SDEMPED), Dallas, TX, USA, 22–25 August 2021; pp. 365–371. [\[CrossRef\]](#)

**Disclaimer/Publisher’s Note:** The statements, opinions and data contained in all publications are solely those of the individual author(s) and contributor(s) and not of MDPI and/or the editor(s). MDPI and/or the editor(s) disclaim responsibility for any injury to people or property resulting from any ideas, methods, instructions or products referred to in the content.